Journal of Applied Physics

Effects of spacer thickness on perpendicular anisotropy L10-FePt/TiN/L10-FePt pseudo spin valves

P. Ho, G. C. Han, K. H. He, G. M. Chow, and J. S. Chen

Citation: J. Appl. Phys. **111**, 083909 (2012); doi: 10.1063/1.3700252

View online: http://dx.doi.org/10.1063/1.3700252

View Table of Contents: http://jap.aip.org/resource/1/JAPIAU/v111/i8

Published by the American Institute of Physics.

Effects of spacer thickness on perpendicular anisotropy $L1_0$-FePt/TiN/$L1_0$-FePt pseudo spin valves

P. Ho,[1,2] G. C. Han,[2] K. H. He,[1] G. M. Chow,[1] and J. S. Chen[1,a)]
[1]*Department of Materials Science and Engineering, National University of Singapore, 117576, Singapore*
[2]*Data Storage Institute, Agency of Science, Technology and Research (A*STAR), 117608, Singapore*

(Received 28 January 2012; accepted 5 March 2012; published online 18 April 2012)

Pseudo spin valves (PSVs) with the structure MgO substrate/$L1_0$-$Fe_{50}Pt_{50}$/TiN/$L1_0$-$Fe_{50}Pt_{50}$ were fabricated with varying TiN spacer thickness from 3 to 7 nm. The giant magnetoresistance (GMR) reached a maximum before diminishing with increasing TiN spacer thickness. The initial enhancement of the GMR was attributed to the reduction in interlayer coupling between the $L1_0$-FePt layers. However, a decline in GMR sets in when the current shunting effects negated the enhancement brought about by the improved decoupling. Magnetostatic coupling was the primary source of interlayer coupling in the PSVs. The dependence of interlayer coupling on the remanent state of the hard $L1_0$-FePt was also examined based on the magnitude and direction of shift in the center of the minor hysteresis loop. While magnetostatic coupling was present in fully saturated hard $L1_0$-FePt, dipolar stray field coupling contributed more significantly to the interlayer coupling strength in partially saturated hard $L1_0$-FePt. The stray field coupling strength depended on both the thickness of the spacer and the density of the reversed domains in the hard $L1_0$-FePt. © *2012 American Institute of Physics*. [http://dx.doi.org/10.1063/1.3700252]

I. INTRODUCTION

The discovery of the giant magnetoresistance (GMR) effect sparked a surge in interest for the integration of spintronics into high-impact technological devices such as the high density hard-disk recording read heads or the emerging magnetoresistive random access memories (MRAM).[1,2] In particular, magnetic trilayers have garnered much scientific interest due to their widespread applications in the rich and growing field of spintronics. The magnetic trilayer system comes in the form of a spin valve, with a non-magnetic (NM) metal spacer sandwiched between two ferromagnets (FM). The GMR phenomenon is attributed to the spin dependent scattering, which occurs in the bulk of the FM, at the FM/NM interfaces, and/or at the surfaces. A difference in the resistance between the parallel and anti-parallel magnetic configuration of the FM constitutes the GMR. The independent switching of the FMs is crucial and this is ensured by the deliberate creation of larger anisotropy energy for the fixed FM or the pinning of the fixed FM using an anti-ferromagnetic layer.

Spin valves were originally developed with in-plane magnetization but systems with high perpendicular magnetocrystalline anisotropy (K_u) have become more attractive due to the demand for greater areal density improvements while maintaining thermal stability.[3–6] $L1_0$-FePt is a suitable candidate for the FM because of its high K_u of 7×10^7 erg/cc. However, the high deposition temperature required of $L1_0$ ordering results in interlayer diffusion within the spin valve. Diffusion within the spin valve affects the interfacial, magnetic and spin transport properties, which in turn adversely impacts the magnetoresistance of the system.[7,8] Hence, it is crucial to adopt spacers with good diffusion barrier properties and/or the ability to lower the deposition temperature of the adjacent $L1_0$-FePt, while being able to sustain the differential scattering within the spin valve. Recently, $L1_0$-FePt based pseudo spin valves (PSVs) with a TiN spacer have been reported.[9] TiN displays excellent diffusion barrier properties and desirable qualities of being chemically stable toward FePt.[10,11] It is also a perpendicular anisotropy inducer, due to the large lattice mismatch of 9.5% between FePt and TiN, which imposes strain ordering on FePt.

The thickness of the spacer layer affects the exchange interactions, such as the magnetostatic interactions through pinholes, Ruderman-Kittel-Kasuya-Yosida (RKKY), Néel and dipolar coupling, between the FM.[12–17] It also influences the extent of current shunting within the PSV. These factors are detrimental to the GMR. A detailed study of the influence of spacer layer thickness on the magnetization reversal and GMR is crucial for a deeper understanding of the $L1_0$-FePt/TiN/$L1_0$-FePt PSV. In this work, we carried out a study on the effects of varying TiN spacer thickness on the crystallographic, magnetic, reversal, interlayer coupling, and magnetotransport properties of the $L1_0$-FePt PSV structures.

II. EXPERIMENT

Samples with the structure $L1_0$-$Fe_{50}Pt_{50}$ (20 nm)/TiN (x nm)/$L1_0$-$Fe_{50}Pt_{50}$ (20 nm) were fabricated on single crystal (001) MgO substrates, with x varied between 3 to 7 nm. The nominal thickness was obtained by calibrating the sputtering parameters with the reference sample. These were prepared using the magnetron sputtering system with a base pressure better than 8×10^{-7} Torr. In all of the samples, the bottom and top $L1_0$-FePtlayers were deposited at 400 and 500 °C, respectively. The TiN spacer was deposited at 350 °C. Crystallographic structures were studied using X-ray diffraction

a)Author to whom correspondence should be addressed. Electronic mail: msecj@nus.edu.sg.

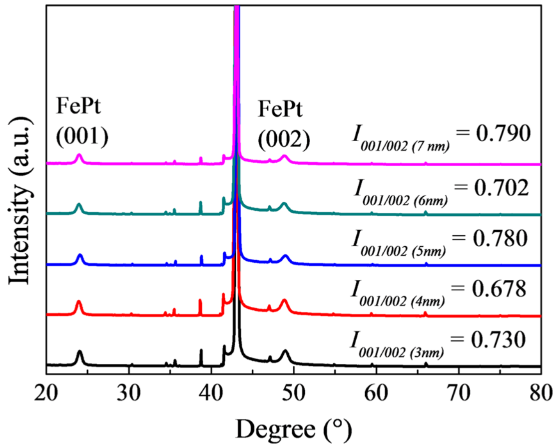

FIG. 1. The XRD spectrum of MgO/$L1_0$-FePt/TiN/$L1_0$-FePt PSVs with TiN spacer thickness of 3, 4, 5, 6, and 7 nm. The unlabeled sharp peaks are inherent of the MgO substrate.

(XRD) with Cu K_α radiation. Focused ion beam (FIB) was used to prepare the sample for high resolution transmission electron microscopy (HRTEM) microstructure analysis. Magnetic properties were characterized by the vibrating sample magnetometer (VSM). Current-in-plane (CIP) resistance measurements were made using a four point probe in the presence of a perpendicular-to-plane field. Surface roughness and magnetic domain configurations were probed using the atomic force microscopy (AFM) and magnetic force microscopy (MFM), respectively. First principles calculations of the band structures were performed using the Vienna *ab* initio simulation package (VASP).[18]

III. RESULTS AND DISCUSSION

The XRD results show similar FePt (002) fundamental and FePt (001) superlattice peaks in all of the PSVs of varying TiN spacer thickness (Fig. 1). Their integrated intensity ratios $I_{(001)}/I_{(002)}$ lie in the range of 0.68 to 0.79.[19] The absence of TiN (002) reflection in the XRD was attributed to the thin TiN spacer that was unable to produce a significant XRD signal beyond the noise level. In addition, TiN possessed a (002) Bragg angle that was close to that of MgO, resulting in its negligible signal being overshadowed by the strong MgO reflection. Figure 2(a) shows the cross-sectional selected area electron diffraction (SAED) pattern along a ⟨001⟩ zone axis for the PSV with TiN spacer thickness of 5 nm. The (001) and (002) FePt spots were aligned with the strong (002) MgO spots. The cross-sectional HRTEM image in Fig. 2(b) shows a highly contrasted TiN spacer and FePt layers due to the large difference in their atomic numbers. The observation of lattice fringes in the FePt and TiN layers ascertained the epitaxial growth of (001) textured FePt and (002) TiN crystalline films.

The magnetization hysteresis loop of the bottom $L1_0$-FePt deposited at 400 °C exhibits a coercivity of 1.8 kOe [Fig. 3(a)]. In all of the PSVs, the top $L1_0$-FePt showed a larger coercivity (H_c) due to a higher K_u, which arose from the higher deposition temperature condition [Figs. 3(b)–3(f)]. The bottom $L1_0$-FePt behaved as the softer free layer while the top $L1_0$-FePt the harder fixed layer of the $L1_0$-FePt/TiN/$L1_0$-FePt PSVs. With increasing TiN spacer thickness, the PSVs became increasingly well-decoupled [Figs. 3(b)–3(f)], exhibiting a larger difference in the H_c between the top and bottom $L1_0$-FePt (Table I). This was attributed to a reduction in interlayer coupling strength with a thicker spacer thickness. The interlayer coupling was largely contributed by the magnetostatic effects due to the magnetic dipoles setup within the $L1_0$-FePt layers. Lee *et al.* reported earlier an exponential relationship between the magnetostatic coupling field (H_{stat}) and spacer thickness (t) (Ref. 20)

$$H_{stat} = \frac{\pi^2\gamma^2 M_P}{\sqrt{2}\lambda t_F}\exp\left(\frac{-2\pi\sqrt{2}t}{\lambda}\right), \tag{1}$$

where γ is the peak-to-peak waviness amplitude of the film, λ is the in-plane wavelength of the surface variations, M_p is the magnetization of the fixed layer, and t_F is the thickness of the free layer. M_p did not vary significantly while t_F was kept constant across the PSVs with varying thickness. In addition, as seen in Table I, the root mean square roughness (R_{RMS}) of the spacer did not vary significantly with thickness. With the same degree of roughness, a smaller TiN thickness resulted in a more significant contribution from the magnetostatic coupling, thus preventing the independent switching of the $L1_0$-FePt layers. Another minor contribution could presumably arise from the direct coupling due to pinholes. Pinhole defects can be thought of as localized regions where the roughness was greater than the thickness of the spacer, hence resulting in physical gaps that promoted direct interactions between the FMs. Pinhole defects were likely to

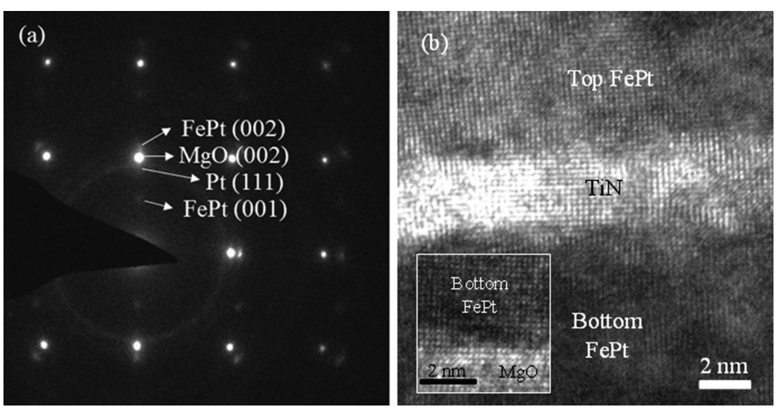

FIG. 2. (a) Cross sectional SAED in the <001> zone axis. The faint ring pattern is the Pt (111) protective layer deposited on the PSV during FIB preparation. (b) Cross sectional HRTEM image for the MgO/$L1_0$-FePt/TiN/$L1_0$-FePt PSV with 5 nm of TiN spacer thickness. Inset shows the HRTEM image of bottom $L1_0$-FePt on MgO substrate.

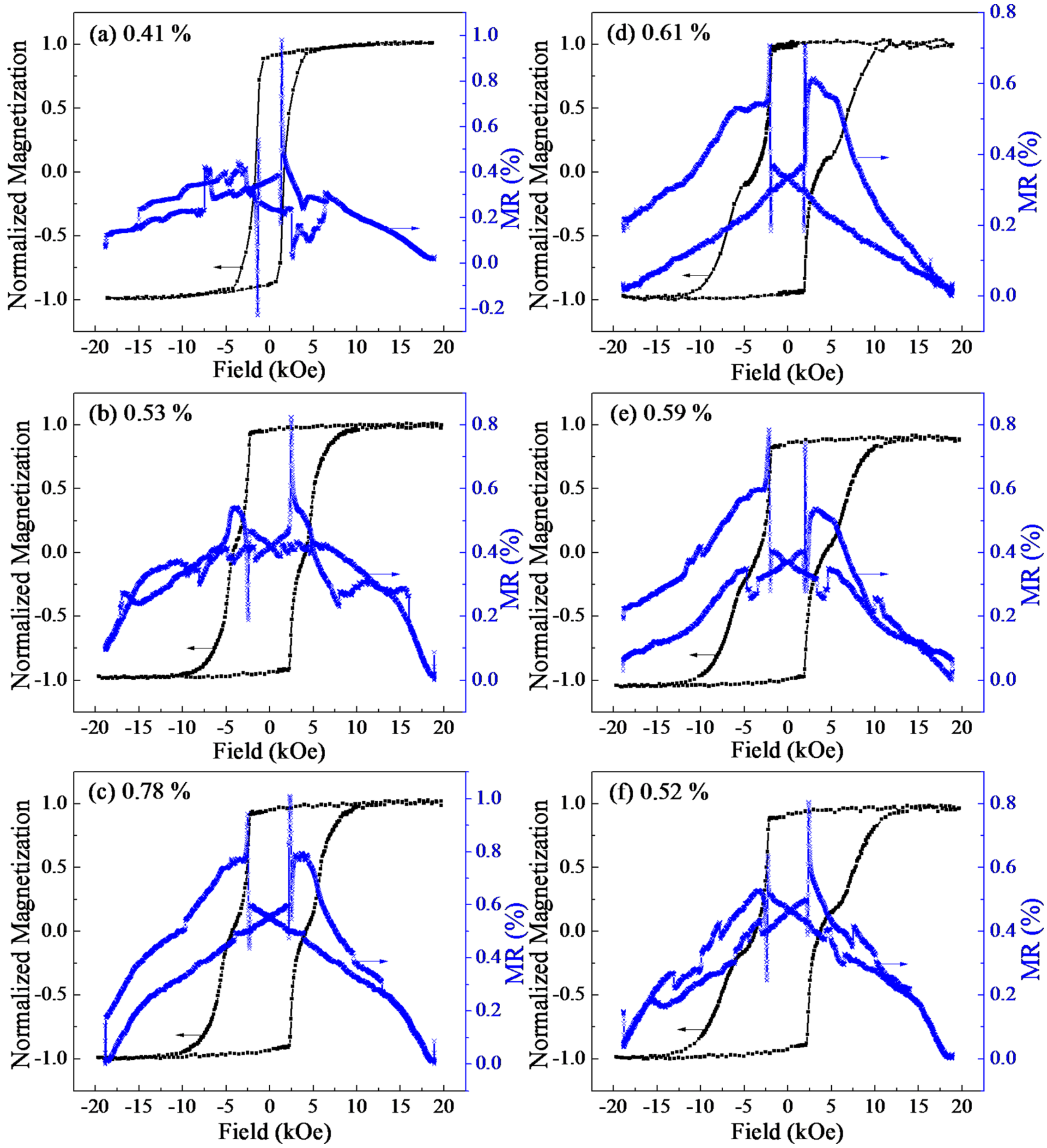

FIG. 3. Out-of-plane magnetization (■) and magnetoresistance (x) curves measured at room temperature for (a) MgO/$L1_0$-FePt, MgO/$L1_0$-FePt/TiN/$L1_0$-FePt PSVs with TiN spacer thickness of (b) 3, (c) 4, (d) 5 (e) 6, and (f) 7 nm.

be more prevalent in a thinner TiN spacer, thereby creating a stronger direct interlayer coupling. This is substantiated with the maximum roughness (R_{max}) values in Table I, in which these values generally increased with decreasing spacer thickness. In particular, for TiN spacer thickness of 3 and 4 nm, the maximum roughness was larger than the spacer thickness, thus suggesting the possible presence of pinhole defects. The oscillatory RKKY coupling favors ferromagnetic or anti-ferromagnetic coupling depending on the thickness of the spacer.[21,22] The presence of this oscillatory coupling could not be determined in this range of TiN spacer thickness studied. The RKKY coupling is understood to have originated from the quantum interference of electrons confined within the non-magnetic spacer. Thus, its strength is typically dominant at spacer thickness of several monolayers. With increasing spacer thickness to a length scale of several nanometers (>3 nm), the RKKY coupling strength diminishes drastically. As such, contribution to the interlayer coupling by RKKY was assumed to be negligible in the PSVs in this work.

TABLE I. A summary of the properties of the MgO/$L1_0$-FePt/TiN/$L1_0$-FePt PSVs with varying TiN spacer thickness of 3 to 7 nm.

TiN thickness (nm)	$H_{c(soft)}$ (kOe)	$H_{c(hard)}$ (kOe)	R_{RMS} (nm)	R_{max} (nm)	GMR (%)	Actual GMR (%)
3	2.60	5.14	0.27	6.44	0.53	0.12
4	2.57	5.98	0.28	5.58	0.78	0.37
5	2.30	7.55	0.30	4.46	0.61	0.20
6	2.28	7.52	0.26	3.75	0.59	0.18
7	2.44	8.23	0.29	4.82	0.52	0.11

The reversal mechanism of both top and bottom $L1_0$-FePt layers in the PSV with TiN spacer thickness of 5 nm is shown in Fig. 4. The remanent magnetic configurations of both $L1_0$-FePt layers were studied at the intermediate stages of their reversal process. A +20 kOe field was first applied to fully saturate the sample. Subsequently, a field between 0 to −12 kOe was applied. MFM images were then taken at zero field to study the remanent magnetic configurations of the layers at different magnetization stages along the first half of the hysteresis loop. Figures 4(b)–4(d) capture the remanent magnetic configurations of the soft bottom $L1_0$-FePt during its various reversal stages. At a field of −6 kOe, complete reversal of the soft bottom $L1_0$-FePt was expected. Figures 4(e)–4(h) depict the remanent magnetic configuration of the hard top $L1_0$-FePt at its various reversal stages. The reversal in both $L1_0$-FePt layers proceeded by reversed domain nucleation and propagation. Their initial reversals were marked by bright white regions, where distinct regions of spin up and spin down configurations were present. As the reversal proceeded to complete saturation in either $L1_0$-FePt layer, the intensity of the reversed domains changed from bright white to a darker yellow as the difference in magnetization between the neighboring domains became less distinct. The reversed domains in the hard top $L1_0$-FePt appeared to be smaller than the soft bottom $L1_0$-FePt. The domain wall width (δ) is related to the K_u by the following relationship $\delta = \pi\sqrt{(A/K_u)}$, where exchange constant $A = 10^{-6}$ erg cm^{-1}.[23] The higher K_u of the top $L1_0$-FePt gave rise to a smaller domain wall width. As such, it was likely that the magnetic domains experienced more efficient pinning by defects compared to the softer bottom $L1_0$-FePt, thus leading to smaller domain sizes.

The influence of the interlayer coupling on the reversal of the $L1_0$-FePt was demonstrated through the shift in the center of the minor hysteresis loops for the PSV with TiN thickness of 5 and 7 nm [Fig. 5(a)]. A +20 kOe field was applied to fully saturate both $L1_0$-FePt layers in the same spin down direction. A field in the range of 0 to −20 kOe was then applied to attain different magnetization states of the hard top $L1_0$-FePt. A minor loop below the switching field of the hard magnetic layer, between +5 to −5 kOe, was then cycled. The difference between the H_c in the first and second quadrants of the minor loop was termed the interlayer coupling field H_{int}.

At an applied field of 0 [Fig. 5(b)] and −20 kOe [Fig. 5(e)] where the hard top $L1_0$-FePt was fully saturated, the shift observed in the minor loop was an indication of the influence of interlayer coupling of the hard and soft $L1_0$-FePt layers due to the presence of magnetostatic coupling. At an applied field of 0 kOe, the hard top $L1_0$-FePt was fully saturated in the spin down configuration. When the minor loop was cycled from +5 to −5 kOe, the soft bottom $L1_0$-FePt had to overcome the interlayer interactions from the hard top $L1_0$-FePt to attain an anti-parallel configuration [inset of Fig. 5(b)]. This resulted in the shift in H_{int} in the negative direction. Conversely, a positive H_{int} was observed at an applied field of −20 kOe, where the soft bottom $L1_0$-FePt reversed more easily to the same parallel configuration as the hard top $L1_0$-FePt with the assistance of the interlayer interactions [inset of Fig. 5(e)].

There was a decrease followed by a peak in H_{int} in the region of applied field of −6 to −10 kOe [Fig. 5(a)]. Figures 4(e)–4(g) discussed earlier show that partially reversed states of the hard top $L1_0$-FePt were present in this region. As such, apart from the magnetostatic effect, dipolar stray field due to the non-uniformly magnetized hard top $L1_0$-FePt film also played a major role in influencing the H_{int}.[24,25] The direction

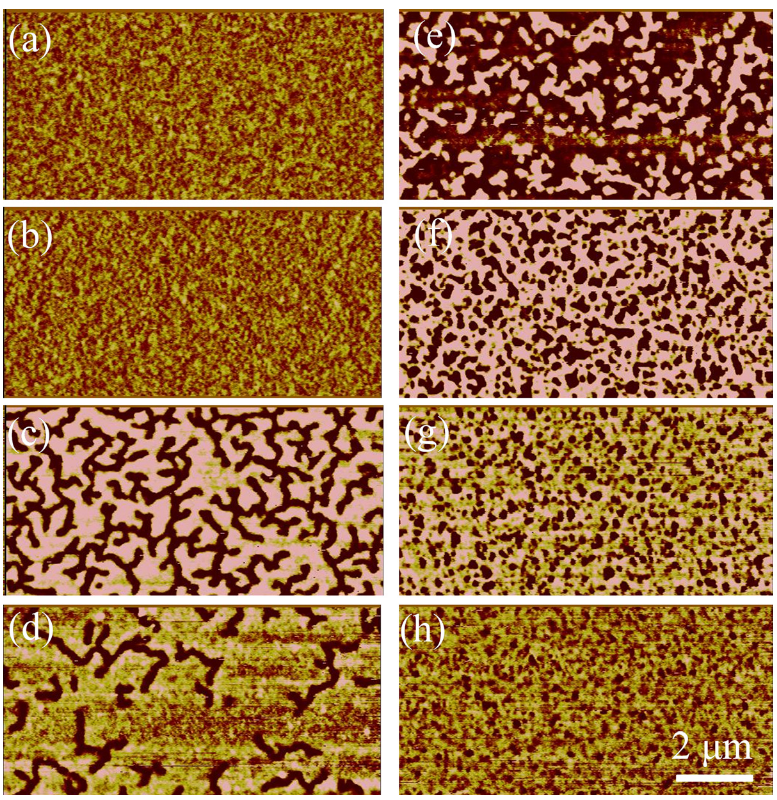

FIG. 4. $10 \times 5\,\mu m^2$ MFM images showing the magnetization states of the $L1_0$-FePt layers in the PSVs with applied field of (a) 0, (b) −2, (c) −3, (d) −4, (e) −6, (f) −8, (g) −10, and (h) −12 kOe. Brighter regions are reversed domains with spin up configuration.

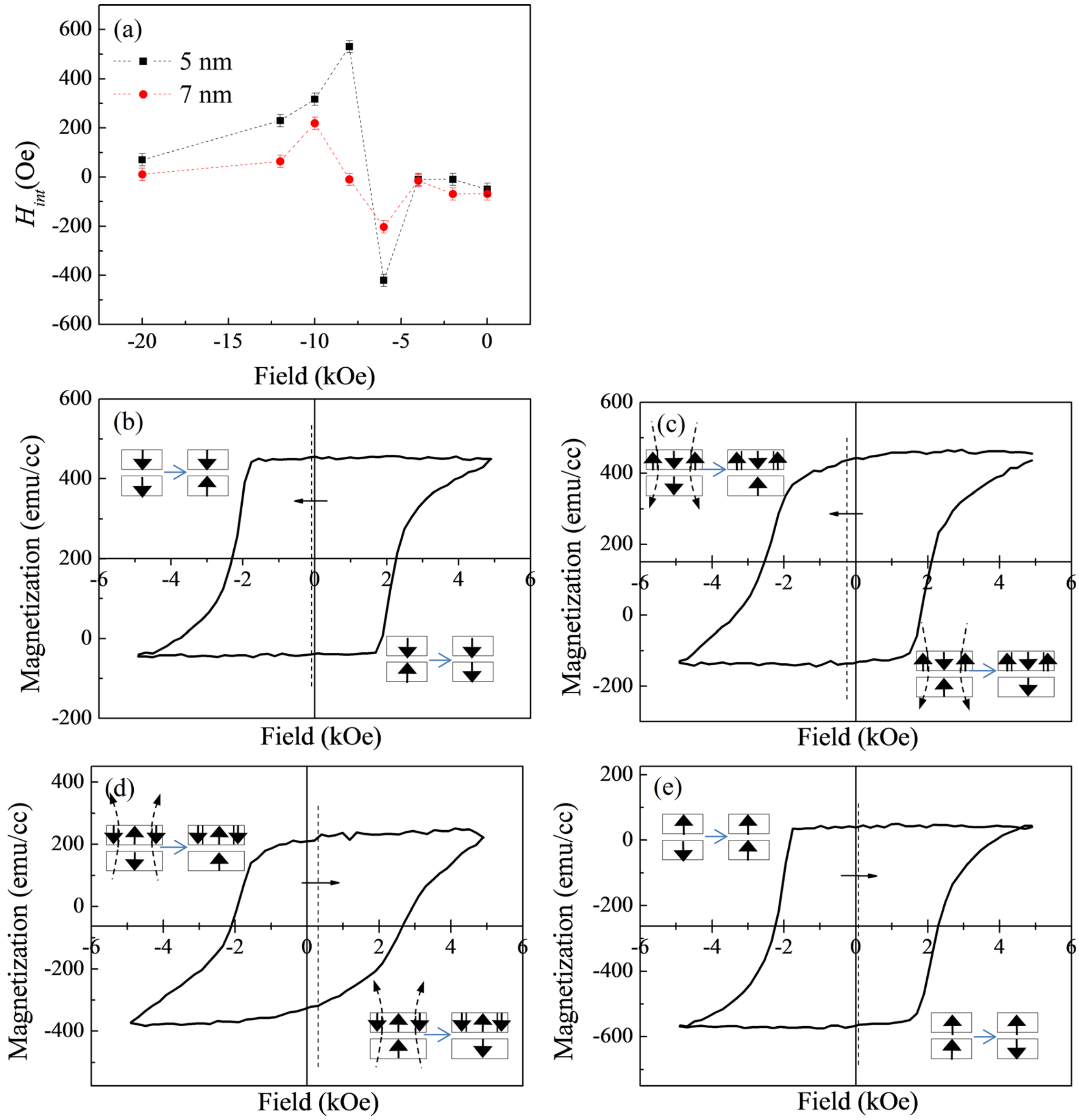

FIG. 5. (a) Interlayer coupling field H_{int} of the minor hysteresis loop vs applied field for the PSVs with TiN spacer thickness of 5 and 7 nm. Dashed lines serve as a guide for the eyes. The vertical error bar represents the systematic instrumental error due to the finite step size of the minor loop. Minor hysteresis loops of the PSV with TiN thickness of 5 nm recorded under the influence of the different magnetization states of the top $L1_0$-FePt, created through applied field of (b) 0 (c) −6 (d) −8, and (e) −20 kOe. The dotted line indicates the center of the minor hysteresis loop; the arrow indicates the direction of the shift of the minor hysteresis loop. Insets indicate schematically the influence of bottom $L1_0$-FePt on the reversal of top $L1_0$-FePt.

and strength of the stray field depended on the density of reversed domains present in the hard top $L1_0$-FePt. At an applied field of −6 kOe, reversed domains with spin up configuration began to nucleate but the density of unreversed domains with spin down configuration remained larger in the hard top $L1_0$-FePt [Fig. 4(e)]. This resulted in a larger extent of dipolar coupling stray field emanating from the walls of the unreversed domains, which impeded the propagation of the reversed domains in the soft bottom $L1_0$-FePt when the minor loop was swept from +5 to −5 kOe [inset of Fig. 5(c)]. Thus, a decrease in H_{int} was observed at an applied field of −6 kOe. However, with an increased applied field of −8 kOe, the proportion of reversed domains with spin up configuration surpassed that of the unreversed domains in the hard top $L1_0$-FePt [Fig. 4(f)]. A positive peak in H_{int} occurred as a result of the fringing fields from the walls of the high density reversed domains, which reduced the local nucleation field and promoted propagation of reversed domains in the adjacent soft bottom $L1_0$-FePt, when the minor loop was swept from +5 to −5 kOe [inset of Fig. 5(d)]. With increasing negative applied field, the increasingly saturated hard top $L1_0$-FePt generated fewer stray fields and the effects of dipolar coupling gradually diminished.

The H_{int} values obtained from the minor loops of the PSV with TiN thickness of 5 and 7 nm are shown in Fig. 5(a). The minor loops of the PSV with TiN thickness smaller than 5 nm were not compared here as fully saturated minor loops were unobtainable. A sufficiently large field range to saturate the minor loop could not be achieved in these poorly decoupled PSVs without capturing the magnetization loop of the hard top $L1_0$-FePt. With a thicker TiN spacer, the reduced interlayer coupling strength between the $L1_0$-FePt layers was reflected with H_{int} values, which were closer to zero, indicating a greater extent of independent reversal of the soft bottom $L1_0$-FePt.

A single layer of bottom $L1_0$-FePt shows a linear behavior of resistivity with magnetic field, displaying a MR of 0.41% [Fig. 3(a)]. At finite temperatures, the directions of the localized d electrons spins fluctuated and the s electrons coupled to them scattered from their inhomogeneous exchange potential.[26,27] This spin flip scattering contributed to the resistivity of the $L1_0$-FePt film. The linear decrease in resistivity occurred with increasing applied field, which acted to suppress the spin disorder scattering. In addition, the spike followed by sharp drop in resistivity at the coercive field of the $L1_0$-FePt film was contributed by magnon magnetoresistance (MMR).[28] At an applied field slightly smaller than the coercive field, the applied field acted in an opposite direction from the magnetization direction. The destabilization of the magnetization direction led to a surge in magnon population, thus bringing about an upsurge in MMR. The magnon population decreased sharply when the applied field and magnetization direction acted in the same direction at the coercive field. Consequently, a reduction in MMR was observed.

Similar contributions by spin disorder and MMR were observed in the MR loops of the PSVs with different TiN thicknesses [Figs. 3(b)–3(f)]. However, the effects of MMR were not prominent at the coercivity of the hard top $L1_0$-FePt, compared to the soft bottom $L1_0$-FePt, due to its larger switching field distribution. At an applied field slightly smaller than the coercive field of the hard top $L1_0$-FePt, a considerable number of spins had already reversed and the remaining spins that could contribute to the MMR effect was significantly reduced. The electron mean free path for TiN is in the range of 39 to 41 nm, which is large enough for the electrons to pass through all the layers successfully when the current flows in the plane of the layers.[29] As such, in addition to the spin disorder and MMR contributions, resistivity due to the spin dependent scattering of the conduction electrons at the trilayer interfaces was also present. The actual GMR contributed by the spin dependent scattering at the interfaces of the $L1_0$-FePt/TiN/$L1_0$-FePt PSV was obtained by subtracting the slope of the background $L1_0$-FePt layer contribution (Table I).[30] With increasing TiN spacer thickness, the actual GMR reached a maximum and then decreased with further increase of TiN thickness (Fig. 6). The initial increase in GMR with an increase in TiN thickness was the result of a reduction in the short-range interlayer magnetostatic interaction. This permitted a difference in the coercivity between the top and bottom $L1_0$-FePt as well as an increase in the effectively decoupled regions, increasing the sample area over which a high resistance anti-parallel configuration of the PSV may be realized. However, with a further increase in TiN thickness, the GMR gradually declined despite a more effectively decoupled PSV and a further reduction of the interlayer coupling strength. Further increasing the spacer thickness increased the probability of conduction electrons being channeled away from the $L1_0$-FePt/TiN interface and confined within the TiN spacer. Due to this current shunting effect, the GMR eventually diminished at larger TiN spacer thickness.

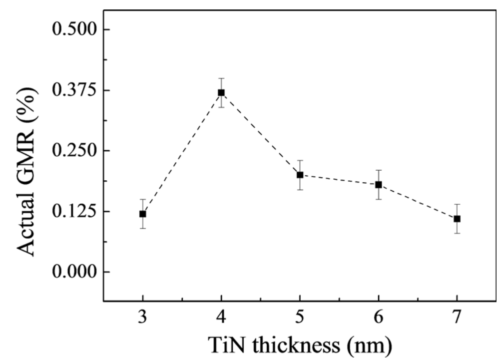

FIG. 6. Actual GMR ratio of MgO/$L1_0$-FePt/TiN/$L1_0$-FePt PSVs with respect to different TiN spacer thicknesses. Dashed line serves as a guide for the eyes. The error bar indicates the standard deviation of 3 independent measurements.

The GMR observed with the TiN spacer was smaller than with the use of metallic spacers such as Ag (1.1%) in similar (001) textured $L1_0$-FePt based PSVs.[4] Based on the resistor model for CIP GMR illustrated in Eq. (2), the magnetoresistance ratio of a multilayer with spacer layer of finite resistance is given by[31]

$$\frac{\Delta R}{R} = \frac{(\alpha - 1)^2}{4\left(\alpha + \frac{\rho d_{NM}}{d_{FM}}\right)\left(1 + \frac{\rho d_{NM}}{d_{FM}}\right)}, \quad (2)$$

where α is the scattering spin asymmetry, d_{NM} is the thickness of the non-magnetic spacer, and d_{FM} is the thickness of the ferromagnet. ρ is the resistivity defined by $\rho_{NM}/\rho_{\uparrow}$, where ρ_{NM} is the resistivity of the non-magnetic spacer, and $\rho_{\uparrow}$ is the majority spin resistivity. It should be noted that this is a largely simplified resistor model that is only applicable for spacer thickness d_{NM} smaller than its electron mean free path. Assuming that the PSVs with various spacer materials possessed the same structure with the same d_{NM} and d_{FM}, the CIP GMR of the PSV would then be largely dependent on the scattering spin asymmetry and resistivity of the spacer. Thus, the smaller GMR in the $L1_0$-FePt/TiN/$L1_0$-FePt PSV was possibly due to the larger resistivity of TiN (15 $\mu\Omega$ cm) compared to Ag (1.6 $\mu\Omega$ cm),[32] which led to a greater extent of spin independent scattering. Another possible reason is the smaller scattering spin asymmetry of TiN with FePt compared to Ag with FePt. Near the Fermi energy level of 0 eV, the energy band structures of TiN and Ag displayed better band structure matching with the FePt spin up electrons [Figs. 7(a) and 7(c)] compared to the FePt spin down electrons [Fig. 7(b) and 7(d)]. This indicates a higher transmission of the majority spin up electrons and a poorer transmission of minority spin down electrons at both the FePt/TiN and FePt/Ag interfaces. The scattering spin asymmetry is the difference in the conductivities (σ) of these two spin channels, where $\alpha = \sigma_{\uparrow}/\sigma_{\downarrow}$. When the $L1_0$-FePt layers were aligned, the majority spin up electrons passed through relatively easily, giving a low resistance state. A higher resistance state was produced when the $L1_0$-FePt layers were anti-aligned and electrons in both channels were reflected at either one of the interfaces. As such, to attain a larger GMR, a larger spin scattering asymmetry would be desirable. The band structures of Ag with FePt spin up

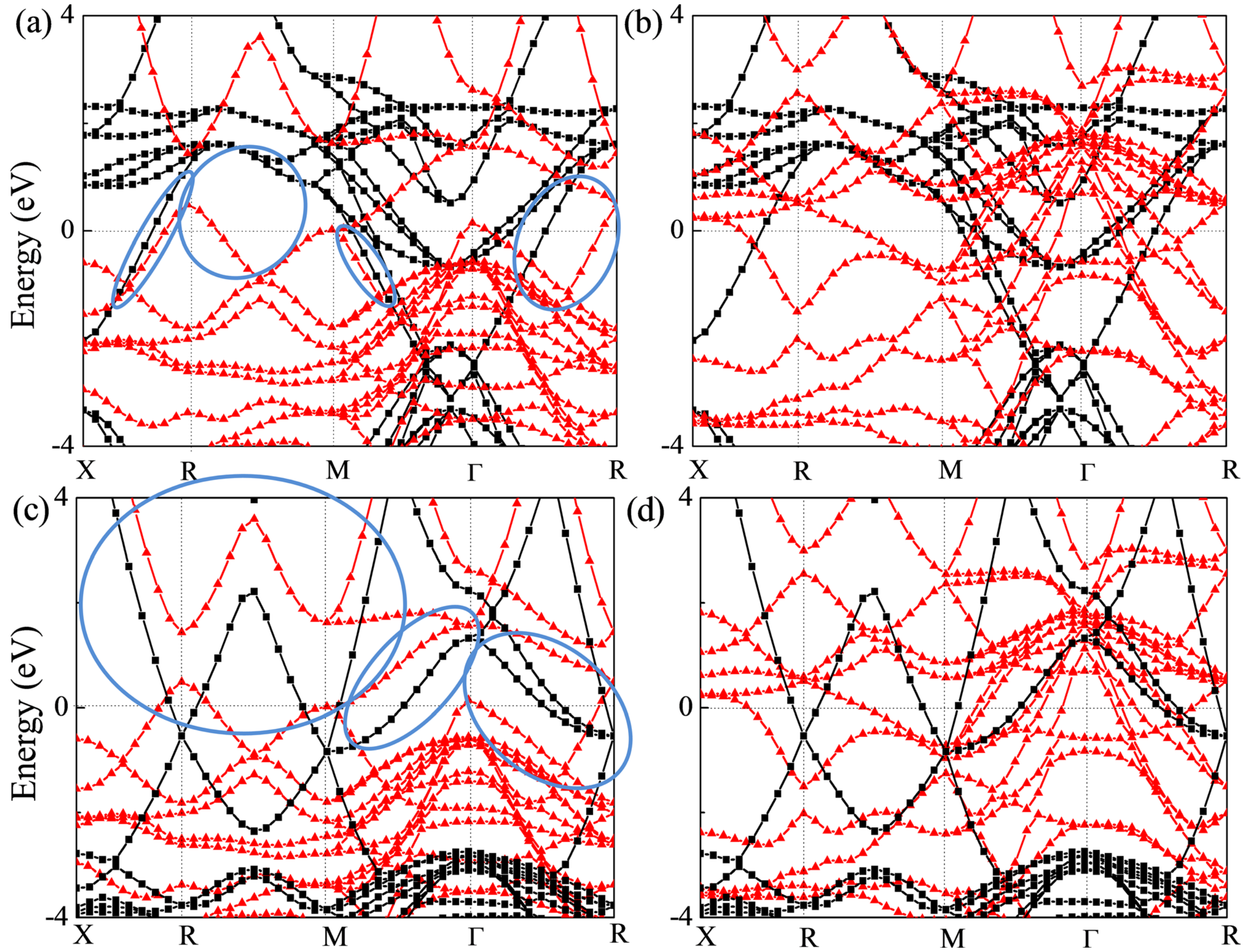

FIG. 7. The energy bands for (a) TiN (■) with spin up FePt (▲), (b) TiN (■) with spin down FePt (▲), (c) Ag (■) with spin up FePt (▲) and (d) Ag (■) with spin down FePt (▲).

electrons [Fig. 7(c)] displayed better band compatibility, with larger regions of similar energy and slope, compared to that of TiN with FePt spin up electrons [Fig. 7(a)]. This suggests the presence of a larger density of states available for the majority spin up electrons at the FePt/Ag interface compared to that of FePt/TiN. The lower GMR observed in the $L1_0$-FePt PSV with TiN spacer could thus be a result of its smaller interfacial scattering spin asymmetry.

IV. SUMMARY

The GMR of the $L1_0$-FePt/TiN/$L1_0$-FePt PSV was strongly dependent on the TiN spacer thickness. The GMR increased to a peak before diminishing with increasing TiN spacer thickness. The initial enhancement of the GMR was attributed to the reduction in interlayer coupling between the $L1_0$-FePt layers. The interlayer coupling was contributed largely by the magnetostatic coupling. However, a decline in GMR set in when the current shunting effects offset the enhancement brought about by the improved decoupling with increasing TiN spacer thickness. The presence of dipolar stray field as well as magnetostatic coupling was also demonstrated through the study of the shift in the center of the minor loops. The reduction in the magnitude of the H_{int} in the minor loops with a thicker TiN spacer reaffirmed the fact that the interlayer coupling strength reduced with increasing spacer thickness.

ACKNOWLEDGMENTS

This work was partially supported by Agency of Science, Technology and Research (A*STAR), Singapore, SERC Grant- 092-156-0118, and Ministry of Education, Singapore, Tier 1 Funding-T11-1001-P04. The authors would like to thank Wintech Nano-technology for providing their technical expertise and quality results for TEM.

[1]S. M. Thompson, J. Phys. D: Appl. Phys. **41**, 093001 (2008).
[2]J. G. Zhu, Proc. IEEE **96**, 1786 (2008).
[3]P. de Person, P. Warin, M. Jamet, C. Beige, and Y. Samson, Phys. Rev. B **76**, 184402 (2007).
[4]P. Ho, G. C. Han, R. F. L. Evans, R.W. Chantrell, G. M. Chow, and J. S. Chen, Appl. Phys. Lett. **98**, 132501 (2011).
[5]T. Seki, S. Mitani, K. Yakushiji, and K. Takanashi, Appl. Phys. Lett. **89**, 172504 (2006).
[6]A. P. Mihai, J. P. Attané, L. Vila, C. Beigné, J. C. Pillet, and A. Marty, Appl. Phys. Lett. **94**, 122509 (2009).
[7]P. Ho, G. C. Han, R. F. L. Evans, R. W. Chantrell, G. M. Chow, and J. S. Chen, IEEE Trans. Magn. **47**, 2646 (2011).
[8]P. Ho, G. C. Han, R. F. L. Evans, R. W. Chantrell, G. M. Chow, and J. S. Chen, Appl. Phys. Lett. **99**, 162503 (2011).
[9]P. Ho, G. C. Han, K. H. He, G. M. Chow, and J. S. Chen, Appl. Phys. Lett. **99**, 252503 (2011).

[10]H. H. Li, K. F. Dong, Y. G. Peng, G. Ju, G. M. Chow, and J. S. Chen, J. Appl. Phys. **110**, 043911 (2011).
[11]Y. Tsuji, S. Noda, and S. Nakamura, J. Vac. Sci. Technol. B **29**, 031801 (2011).
[12]S. Wiebel, J. P. Jamet, N. Vernier, A. Mougin, J. Ferre, V. Baltz, B. Rodmacq, and B. Dieny, Appl. Phys. Lett. **86**, 142502 (2005).
[13]W. S. Lew, S. P. Li, L. Lopez-Diaz, D. C. Hatton, and J. A. C. Bland, Phys. Rev. Lett. **90**, 2172011 (2003).
[14]L. Thomas, M. G. Samant, and S. S. P. Parkin, Phys. Rev. Lett. **84**, 1816 (2000).
[15]D. Tripathy, A. O. Adeyeye, and S. Shannigrahi, Phys. Rev. B **75**, 012403 (2007).
[16]N. Thiyagarajah and S. Bae, J. Appl. Phys. **104**, 113906 (2008).
[17]C. L Zha, Y. Y. Fang, J. Nogués, and J. Åkerman, J. Appl. Phys. **106**, 053909 (2009).
[18]G. Kresse and J. Hafner, Phys. Rev. B **47**, 558 (1993); **49**, 14251 (1994).
[19]Y. Liu, D. J. Sellmyer, and D. Shindo, Hand Book of Advanced Magnetic Materials (2006), Vol. 1, p. 199.
[20]C. L. Lee, J. A. Bain, S. Chu, and M. E McHenry, J. Appl. Phys. **91**, 7113 (2002).
[21]P. Bruno and C. Chappert, in *Magnetism and Structure in Systems of Reduced Dimension*, edited by R. F. C. Farrow *et al*. (Plenum, New York, 1993), pp. 389–399.
[22]F. J. Himpsel, J. E. Ortega, G. J. Mankey, and R. F. Willis, Adv. Phys.: Magn. Nanostruct **47**, 511 (1998).
[23]K. M. Seemann, V. Baltz, M. Mackenzie, J. N. Chapman, B. J. Hickey, and C. H. Marrows, Phys. Rev. B. **76**, 174435 (2007).
[24]P. Ho, G. C. Han, G. M. Chow, and J. S. Chen, Appl. Phys. Lett. **98**, 252503 (2011).
[25]V. Baltz, A. Marty, B. Rodmacq, and B. Dieny, Phys. Rev. B **75**, 014406 (2007).
[26]P. Allia, F. Celegato, M. Coisson, P. Tiberto, F. Vinai, F. Albertini, F. Casoli, and S. Fabbrici, J. Magn. Magn. Mater. **322**, 1898 (2010).
[27]J. Yu, U. Rüdiger, A. D. Kent, R. F. C. Farrow, R. F. Marks, D. Weller, L. Folks, and S. S. P. Parkin, J. Appl. Phys. **87**, 6854 (2000).
[28]A. P. Mihai, J. P. Attané, A. Marty, P. Warin, and Y. Samson, Phys. Rev. B **77**, 060401 (2008).
[29]W. Tsai, M. Delfino, J. A. Fair, and D. Hodul, J. Appl. Phys. **73**, 4462 (1993).
[30]C. L. Zha, S. Bonetti, J. Persson, Y. Zhou, and J. Åkerman, J. Appl. Phys. **105**, 07E910 (2009).
[31]E. Y. Tsymbal and D. G. Pettifor, in "Perspective of Giant Magnetoresistance," in *Solid State Physics*, edited by H. Ehrenreich and F. Spaepen (Academic, 2001), Vol. 56, pp. 113–237.
[32]*CRC Handbook of Chemistry and Physics*, 92nd ed., edited by D. R. Lide (CRC, Boca Raton, 2009), Chap. 12, p. 42.